ADVANCED MATERIALS
www.advmat.de

Laser-Induced Hole Coherence and Spatial Self-Phase Modulation in the Anisotropic 3D Weyl Semimetal TaAs

*Yixuan Huang, Hui Zhao, Zhilin Li, Lili Hu, Yanling Wu, Fei Sun, Sheng Meng, and Jimin Zhao**

Laser-induced electron coherence is a fascinating topic in manipulating quantum materials. Recently, it has been shown that laser-induced electron coherence in 2D materials can produce a third-order nonlinear optical response spatial self-phase modulation (SSPM), which has been used to develop a novel all-optical switching scheme. However, such investigations have mainly focused on electron coherence, whereas laser-induced hole coherence is rarely explored. Here, the observation of the optical Kerr effect in 3D Weyl semimetal TaAs flakes is reported. The nonlinear susceptibility ($\chi^{(3)}$) is obtained, which exhibits a surprisingly high value (with $\chi^{(3)}_{\text{one-layer}} = 9.9 \times 10^{-9}$ e.s.u. or 1.4×10^{-16} m^2 V^{-2} at 532 nm). This cannot be explained by the conventional electron mobility, but can be well understood by the unique high anisotropic hole mobility of TaAs. The wind-chime model and $\chi^{(3)}$ carrier mobility correlation adequately explain the results, suggesting the crucial role of laser-induced nonlocal ac hole coherence. These observations extend the understanding of SSPM from 2D to 3D quantum materials with anisotropic carrier mobility and from electron coherence to hole coherence.

1. Introduction

Spatial self-phase modulation (SSPM), which is also known as the optical Kerr effect or ac Kerr effect, is a third-order nonlinear optical effect that significantly differs from the Kerr effect. One of the pioneering discoveries was carried out in a 1D material—nematic liquid crystals, in 1981.[1] Thirty years later, in 2011, SSPM has been investigated in the prototypical 2D material graphene[2] and subsequently, SSPM investigations have been conducted in various 2D materials.[3–7] We proposed and developed an optical switch based on SSPM,[3] which endowed SSPM with great practical application potential. This aroused considerable research interest and resulted in a lot of investigations[8–14] along the innovative direction of all-optical switching[15] based on SSPM.[3]

Significantly, in ref. [3], a laser-induced electronic coherence origin has been innovated for SSPM, which was well explained by a wind-chime model and confirmed by both the ring formation time and optical switching behavior. Further, a comparison between the SSPM in a 0D material C_{60} and layered material graphite flake[4] demonstrated the crucial role of free electron (or other carriers) motion in generating SSPM. Similar confirming results have been observed by comparing the SSPM in 2D black phosphorus flakes with nanoparticles of black phosphorus.[7] Recently, SSPM in $MoTe_2$[5] has been investigated, which indicated that the SSPM nonlinear response is correlated to the electron mobility and effective mass, which further confirmed the electronic origin of SSPM. So far, investigations of the electronic origin of SSPM have been mainly performed using 2D materials and SSPM in 3D materials, and its underlying mechanism have been rarely reported. The 3D material graphite that we investigated[4] is indeed a layered 2D material. Here, we investigate a typical 3D bulk material TaAs to verify the generation of SSPM.

Thetopological material TaAs is a 3D Weyl semimetal that contains 12 pairs of gapless Weyl nodes in the Brillouin zone.[16] In particular, it possesses an ultrahigh hole mobility even at room temperature, with $\mu_{\text{hole}} = 10^4$ cm^2 V^{-1} s^{-1}.[17] TaAs is a polar semimetal with broken centro-inversion symmetry,[18] which leads to prominent second-order nonlinear optical responses, such as strong second harmonic generation[19–21] and optical rectification.[22] These properties make TaAs a promising material for terahertz generation[23,24] and optoelectronic devices, including far-infrared detectors.[19] Our group recently investigated the ultrafast quasiparticle dynamics of TaAs (as well as other topological materials[25–31]) and obtained its electron-phonon coupling strength.[25] However, to date, few studies[32] on the third-order nonlinear optical investigation of TaAs have been reported, which may potentially hinder its further application in nonlinear photonics.

In this work, we observe SSPM in TaAs flakes suspended in a *N*-methyl-2-pyrrolidinone (NMP) dispersion. We obtain

Y. Huang, H. Zhao, Z. Li, L. Hu, Y. Wu, F. Sun, S. Meng, J. Zhao
Beijing National Laboratory for Condensed Matter Physics
and Institute of Physics
Chinese Academy of Sciences
Beijing 100190, China
E-mail: jmzhao@iphy.ac.cn
Y. Huang, H. Zhao, Z. Li, S. Meng, J. Zhao
School of Physical Sciences
University of Chinese Academy of Sciences
Beijing 100049, China
S. Meng, J. Zhao
Songshan Lake Materials Laboratory
Dongguan, Guangdong 523808, China
The ORCID identification number(s) for the author(s) of this article can be found under https://doi.org/10.1002/adma.202208362.

DOI: 10.1002/adma.202208362

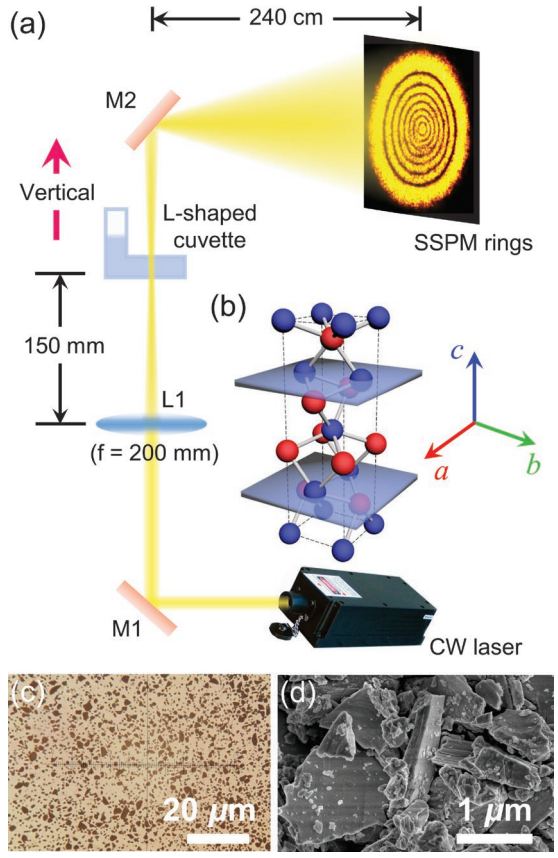

Figure 1. Schematic of the experimental setup, lattice structure, and characterizations. a) Vertical SSPM experimental setup. A Gaussian laser beam is focused into an L-shape cuvette through a convex lens. The diffraction beam forms SSPM patterns on the far-field white screen. b) Light interaction with TaAs. Blue planes: effective layers of hole distribution. c) Microscopy photo of the TaAs flakes. d) SEM image of the TaAs flakes.

the third-order nonlinear optical susceptibility $\chi^{(3)}$ of TaAs at various optical wavelengths ranging from visible light to the near-infrared regime. As expected, the value of $\chi^{(3)}$ is band-dependent. The effective charge layer is identified and the value for an effective one-layer material, $\chi^{(3)}_{\text{one-layer}}$, is estimated. For example, $\chi^{(3)}_{\text{one-layer}}$ at 532 nm is 9.9×10^{-9} e.s.u. (i.e., 1.4×10^{-16} m^2 V^{-2}). Significantly, our experimental results demonstrate the validity of the wind-chime model in explaining the SSPM of this 3D material, owing to its anisotropic carrier mobility. Furthermore, a comparison of its SSPM with other similar quantum materials indicate that the dependence of $\chi^{(3)}_{\text{one-layer}}$ on the carrier mobility (μ-dependence) remain valid for such a hole-based material.

2. Experimental Section

Figure 1a shows the schematic of the experimental setup, which resembles those of previous experiments,[2–6] except that a vertical excitation geometry was used. A linearly polarized continuous wave (CW) laser beam was focused onto the TaAs suspension by a focusing lens whose focal length was 200 mm. The L-shape cuvette containing the TaAs suspension was customized with a height of 10 mm. The distance between the lens and center of cuvette was maintained at 150 mm. During the experiment, concentric conical rings emerged to form SSPM diffraction patterns on a white screen placed 240 cm away from the cuvette. A camera was used to record the entire process of the formation of patterns. The laser beam was directed to pass through the cuvette in a strict vertical direction to eliminate the influence of gravity. Figure 1b schematically shows the lattice structure of TaAs, which possesses a body-centered-tetragonal symmetry, where $a = b = 3.44$ Å and $c = 11.64$ Å.[18] Light propagated along the c-axis. When light interacted with the TaAs crystal, the 3D crystal was aligned such that the ab plane was perpendicular to the light propagation (see discussions in a latter paragraph).

Table 1. Dependence of the $\chi^{(3)}_{\text{total}}$, $\chi^{(3)}_{\text{one-layer}}$ values on the wavelength of the excitation laser, along with the radius of the laser beam used.

λ [nm]	beam radius [mm] before the lens	$\chi^{(3)}_{\text{total}}$ [10^{-4} e.s.u.]	$\chi^{(3)}_{\text{one-layer}}$ [10^{-9} e.s.u.]
405	0.67	6.06	10.50
473	0.78	5.86	10.20
532	0.79	5.68	9.86
589	1.23	5.51	9.56
671	0.77	5.30	9.19
733	0.74	5.14	8.92
800	0.74	4.86	8.44
841	0.74	4.65	8.07

Multiple CW lasers with different wavelengths had been employed to conduct the experiment (Table 1). Identical dispersive suspensions of TaAs flakes in NMP solution were prepared for the different experiments. The size of the TaAs flakes was characterized using microscopy images and scanning electron microscopy (SEM) images (Figure 1c,d). The lateral size of the flakes ranged from 1–5 μm. The concentration of the suspension was optimized to be 0.2 g L^{-1} (i.e., 0.00078 mol L^{-1}) to guarantee that no sample precipitated during the entire experiment. For each measurement, the suspension was sonicated 10 min before the experiment.

3. Results and Discussion

Typical SSPM patterns generated at eight different wavelengths are shown in **Figure 2**a. For the same laser intensity, the number of rings decreases with increasing wavelength. The shape of each pattern is identical to the cross-sectional shape of the corresponding incident laser beams (see Supporting Information). All the patterns remain stable throughout the experiments because our vertical light geometry avoids thermal-convection-induced ring deformation[2] (also known as the gravity effect,[33] see Supporting Information). As shown in Figure 2b, the number and diameter of the SSPM concentric rings linearly increase with the incident laser power and fluence, which is the critical characteristic of the SSPM nature of the patterns.

To obtain the third-order nonlinear optical susceptibility, we plot the ring number N depending on the laser intensity I in

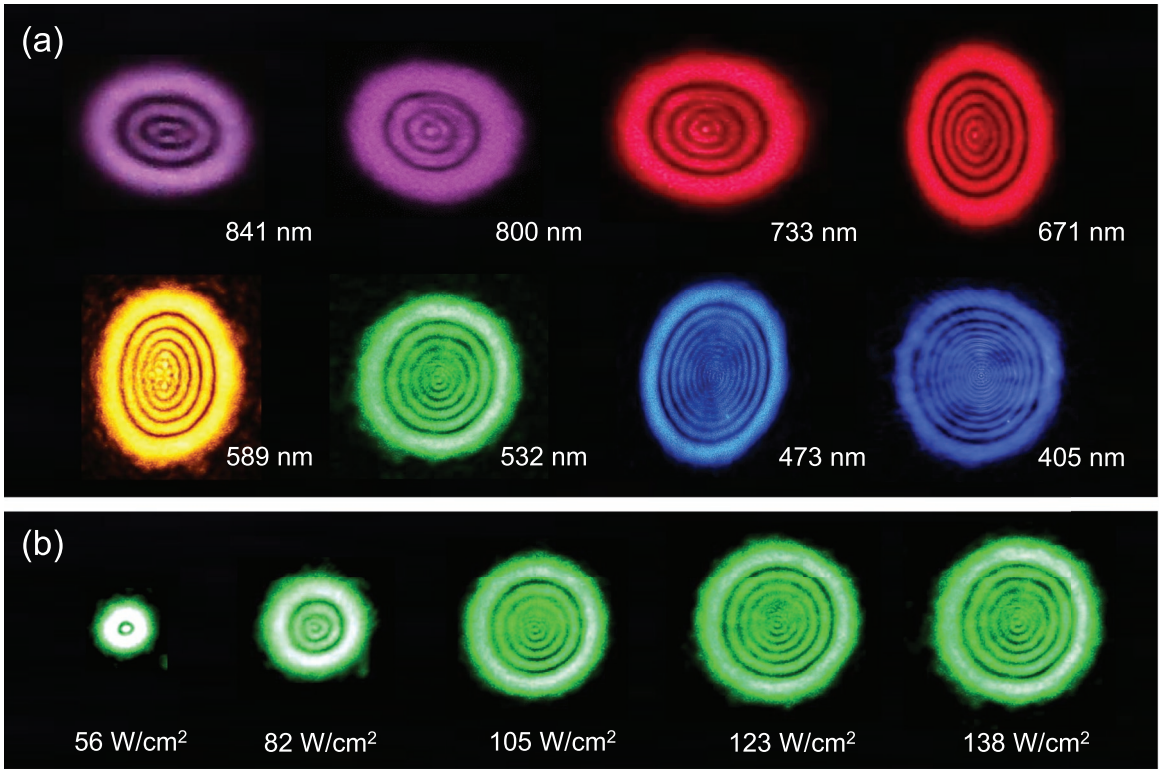

Figure 2. a) Typical SSPM patterns generated by laser beams with wavelengths of 841, 800, 733, 671, 589, 532, 473, and 405 nm. The incident intensity for all the wavelengths is approximately 100 W cm^{-2}. The number of rings decreases with increasing wavelength. b) Both the number and diameter of the concentric rings increase linearly with the incident fluence.

Figure 3a. The dependence exhibits a linear relation between N and I, which can be used to obtain the overall nonlinear optical coefficient:[3]

$$\chi^{(3)}_{\text{total}} = \frac{c\lambda n_0}{2.4\times10^4\,\pi^2 l}\times\frac{dN}{dI} \tag{1}$$

where λ is the laser wavelength, $n_0 = 1.47$ is the refractive index of the NMP solvent, l is the height of the cuvette (here $l = 1$ cm), and c is the light speed in vacuum. In Figure 3a, the linear relation is analyzed for different excitation wavelengths, where the slopes gradually decrease with increasing wavelength. This indicates that the value of $\chi^{(3)}_{\text{total}}$ decreases with increasing wavelength. The values of the overall nonlinear response $\chi^{(3)}_{\text{total}}$ obtained at multiple wavelengths are summarized in Table 1. The overall magnitude is of the order of 5×10^{-4} e.s.u. (i.e., 1×10^{-8} m^2 V^{-2}). The magnified view in the inset of Figure 3a reveals the thresholds for observing the SSPM phenomenon at multiple wavelengths. The threshold monotonously increases with the wavelength, which is similar to that observed in 2D materials.[3]

In ref. [3], a wind-chime model was proposed to explain the formation process of the SSPM pattern. Photon-excited carriers (either electrons or holes) in each flake are correlated by the incident laser pulses through the laser-induced nonlocal ac electron coherence. It is known that TaAs possesses an exceptionally high hole mobility, while its electron mobility is two orders of magnitude smaller.[17] Hence, we interpret that the SSPM in TaAs arises primarily from laser-induced hole coherence.[6] Although possible hole-based SSPM has been mentioned in our previous work,[3] thorough investigations are lacking.

Next we investigate the effective third-order nonlinear susceptibility for one-layer of the material, $\chi^{(3)}_{\text{one-layer}}$, which is meaningful for comparisons among different materials. The wind-chime model provided a way to estimate the $\chi^{(3)}_{\text{one-layer}}$ in 2D layered materials. The key step is to obtain the number of effective layers that the laser beam traverses through. In 2D layered materials, a single layer can be easily defined because unit cell layers are usually separated by the van der Waals force. However, in a 3D material, there is no van der Waals force. Thus, the definition of one layer is not necessarily identical the unit cell layer. A reasonable classification is the effective coherent photocarrier layer. In this work, it is the effective coherent light-generated hole layer. Microscopically, the holes are photogenerated from the covalent Ta—As bonds. The photoexcited holes are free charge carriers in the momentum and real spaces, which do not form charge layers. However, one can still quantitatively estimate the photoexcited hole density in the terms of effective charge layers. As shown in Figure 1b, the laser beam travels through TaAs along the c-axis, whereby each single unit cell layer contributes effectively two layers of holes (marked by the blue plates).

We estimate the number of effective layers based on the calculation we proposed in ref. [3]. From the weight of the TaAs flake powder (12 mg) and volume of the TaAs suspension solution

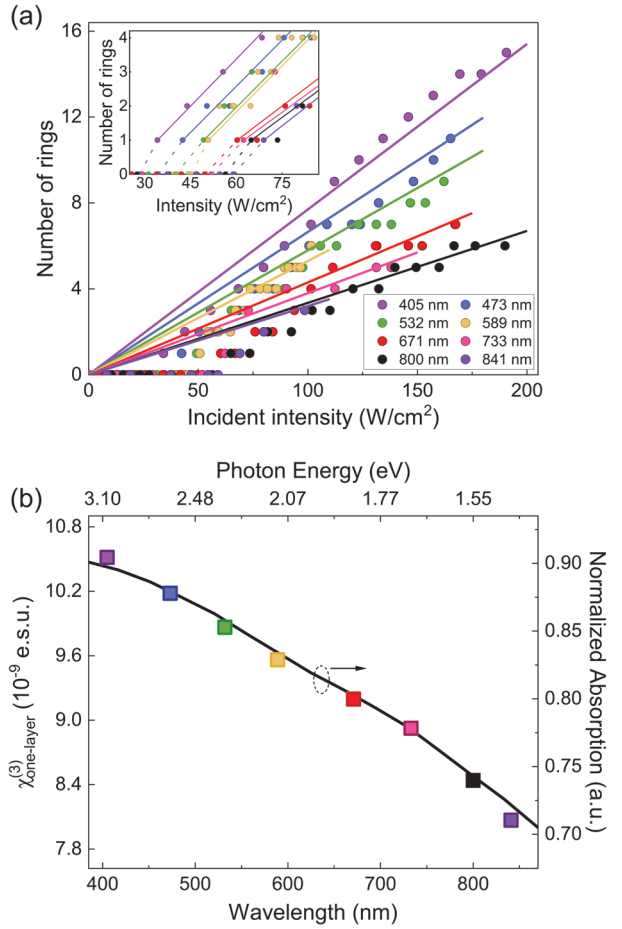

Figure 3. a) Intensity dependence of the number of rings at different wavelengths. The nonlinear optical coefficients $\chi^{(3)}$ are directly interpreted from the slopes. Solid lines: guides for the eye. Inset: Thresholds of the emergence of SSPM patterns at different wavelengths. b) Comparison of the effective one-layer third-order nonlinear optical susceptibility $\chi^{(3)}_{\text{one-layer}}$ and photon absorption spectrum of TaAs. The colored squares represent the $\chi^{(3)}_{\text{one-layer}}$ obtained experimentally. The black curve represents the absorption curve of TaAs, adapted from ref. [34]. The arrow indicates the normalized values of the absorption curve. Adapted with permission.[34] Copyright 2018, Wiley-VCH.

(60 mL, in a separate tube), we find the concentration of our TaAs suspension solution is 0.2 g L^{-1}. Considering the relative molecular mass of TaAs as 256 g mol^{-1}, the mole concentration of our TaAs suspension solution is $\rho = 7.8 \times 10^{-4}$ mol L^{-1}. During the sonication, which takes 3 min, no prominent precipitation is observed. Then a portion of the suspension is transferred into the cuvette. We consider only the horizontal part of the cuvette (i.e., with a volume of $1 \times 1 \times 3$ cm^3). The total number of TaAs primitive cells (each contains four TaAs molecules) in the cuvette is $M = \rho/4 \times V \times N_A$, where V is the volume of cuvette and N_A is the Avogadro constant. The number of primitive cells required to cover an effective layer is the ratio between the lateral area of the cuvette and unit cell area in the *ab* plane (i.e., $m = S_{\text{lateral}}/S_{\text{unit-cell-area-in-}ab\text{-plane}}$). Hence, the number of TaAs unit cell layers that the laser beam traverses through is $N_{\text{cell}} = M/m = 139$, where $V/S_{\text{lateral}} = l = 1$ cm is the height of the cuvette. For each wavelength, the sonication and subsequent experiment take 3 and 5–8 min, respectively. The instability of the suspension for the entire process of 8–11 min may lead to a slight precipitation. We estimate N_{cell} as 120. Thus, the number of carrier layers (N_{carrier}) that the laser beam traverses through is $N_{\text{carrier}} = 2N_{\text{cell}} = 240$.

We have $E_{\text{total}} = N_{\text{carrier}}E_{\text{one-layer}}$ because SSPM is a purely coherent nonlinear process[2] according to the laser-induced electron (carrier) coherence mechanism.[3] This leads to $I_{\text{total}} = N^2_{\text{carrier}}I_{\text{one-layer}}$. Thus, under ideal conditions, $\chi^{(3)}_{\text{total}} = N^2_{\text{carrier}}\chi^{(3)}_{\text{one-layer}}$.[2] Consequently, the values of $\chi^{(3)}_{\text{one-layer}}$ are obtained for the various wavelengths, which are summarized in Table 1 and explicitly shown in Figure 3b. The dependence of $\chi^{(3)}_{\text{one-layer}}$ on wavelength compares well with that of the absorption of TaAs (Figure 3b). The values of $\chi^{(3)}_{\text{one-layer}}$ and absorption are proportional. This phenomenon is wholly consistent with the laser-induced electron coherence mechanism;[3] however, here it is laser-induced hole coherence instead. Because TaAs is a semimetal, each of the eight visible-to-near infrared cw laser beams employed in the experiment generates holes through dipole transitions (i.e., two photon excitation SSPM is unlikely to occur here).

It is interesting to consider the connection between the laser-induced hole coherence and topological properties of the material. The dispersion of $\chi^{(3)}_{\text{one-layer}}$ for TaAs is consistent with the optical measurements of its bulk electronic states[34,35] (Figure 3b). In the presence of spin-orbit coupling, the band of TaAs close to the Fermi level in the bulk Brillouin zone is gapped, except for being connected by the 12 pairs of Weyl cones.[36] Upon excitation by large energy photons, interband transitions can occur between massless Weyl cone states and massive bulk states.[23] Such photoexcited carriers mainly relax by traversing in the momentum space into the Weyl cones, and then decaying by nonradiative recombination across the Weyl points. During this process in the Weyl cones, the carriers assume the Weyl properties, such as very high hole mobility (thus very large value of $\chi^{(3)}$). This is much faster than the recombination through across-gap radiative transition.[37] Hence, more photoexcited carriers traverse into the Weyl cones and participate in the SSPM process than it appears if only the intraband damping without phonon scatterings is considered (see Supporting Information). Because the interaction time of the hole-phonon scattering is significantly longer than that of hole-hole scattering,[37] the former has a greater effect on the value of $\chi^{(3)}$. Note that all free carriers, including the Weyl cone carriers, contribute to the SSPM. Thus, the large $\chi^{(3)}$ nonlinearity observed is connected with the Weyl properties (see Supporting Information). Similar observation of nonlinear response owing to the W1 and W2 Weyl nodes fermions has also been investigated in ref. [32]. In this case, electronic doping is not extensive and the laser power is not extremely high. Hence, the conduction band carrier density is far less than creating Pauli blocking.[32,38]

Furthermore, we investigate the correlation between $\chi^{(3)}_{\text{one-layer}}$ and the carrier mobility (i.e., the μ-dependence). A positive correlation between the two quantities has been reported in ref. [5] for 2D materials. Although a tentative linear relation has been suggested there, it might be verified in future, because the

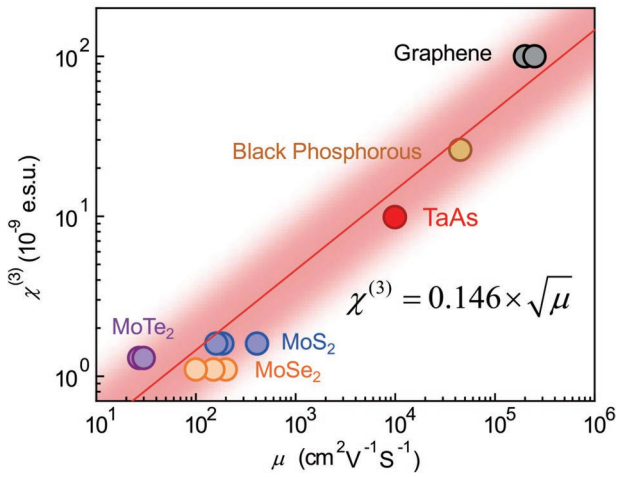

Figure 4. Positive correlation between $\chi^{(3)}_{\text{one-layer}}$ and carrier mobility μ for 2D layered materials and 3D TaAs. All the values except those for TaAs are adapted from ref. [5]. Red stripe: positive correlation. Red line: Tentative concrete linear relation as a visual guide. Adapted with permission.[5] Copyright 2019, Optical Society of America.

complete dependence includes other quantities as well. The empirically fitted relation reads

$$\chi^{(3)}_{\text{one-layer}} = 0.146 \times \sqrt{\mu} \tag{2}$$

where μ is the carrier mobility. As mentioned previously, we use the hole mobility in Equation (2). The value is roughly $\mu_{\text{hole}} = 9 \times 10^3$ cm^2 V^{-1} s^{-1} at room temperature.[17,32] We plot the result of TaAs thus obtained in **Figure 4**, where the results for all the other materials are adapted from ref. [5]. The properties of TaAs fit in the positive correlation relation (marked by the broad red stripe) well, although the other materials are 2D materials. So far, the value of the effective hole mass has not been reported for TaAs. Hence, we cannot further investigate the correlation between $\chi^{(3)}_{\text{one-layer}}$ and the effective mass. From Figure 1a, the average thickness of our TaAs flakes is ≈40 nm, corresponding to about 35 layers of unit cells. Hence, the flakes can be considered as bulk samples. The influence of dielectric environment change on the hole mobility is negligible.

Finally, we investigate the emergence process of the SSPM patterns. Snapshots of the pattern formation process, obtained using laser beams at different wavelengths, are recorded (**Figure 5**a). The fluence of each laser beam is maintained at 90 W cm^{-2}. The ring diameters and ring numbers both increase monotonously with time. The time scale required for ring pattern formation is of the order of 1 s. The time evolution of the SSPM patterns can be adequately described by the wind-chime model.[3] This yields the formation time of the SSPM pattern as

$$\mathcal{T} = \frac{\varepsilon_r \pi \eta \xi R c}{1.72(\varepsilon_r - 1) I h} \approx 0.87 \text{ s} \tag{3}$$

where c is the speed of light, $\varepsilon_r \approx 8.7$ is the average relative dielectric constant of TaAs,[38] $\eta = 1.7 \times 10^{-3}$ Pa s is the viscous coefficient of the solvent NMP, and $\xi \approx 0.1$ in our experiment. By estimating the average thickness and radius of the TaAs flakes to be $h \approx 0.04$ and $R \approx 0.7$ μm, respectively, we determine the theoretical time for ring pattern formation to be ≈2.0 s. Experimentally, the ring formation process obeys an exponential growth model as noted in ref. [5], as $N = N_{\max}(1 - e^{-t/\tau_{\text{rise}}})$. Here, τ_{rise} is the rise time for ring formation, which is different from the ring pattern formation time T.[5] From the fitting results in Figure 5b, we estimated that T = 2.5 s and τ_{rise}=0.59 s. The value of T is of the same order as the calculated value (≈2.0 s) (Equation (3)). This discrepancy may be explained by the rough estimation of the factor ξ or the definition of the ring pattern formation time in Figure 5b. The values of T and τ_{rise} at the three wavelengths are close to each other, owing to the nearly constant relative dielectric constant of TaAs in this wavelength region.[39] Overall, the wind-hhime model originally proposed for 2D materials remains valid for this 3D material preserving high isotropic mobility.

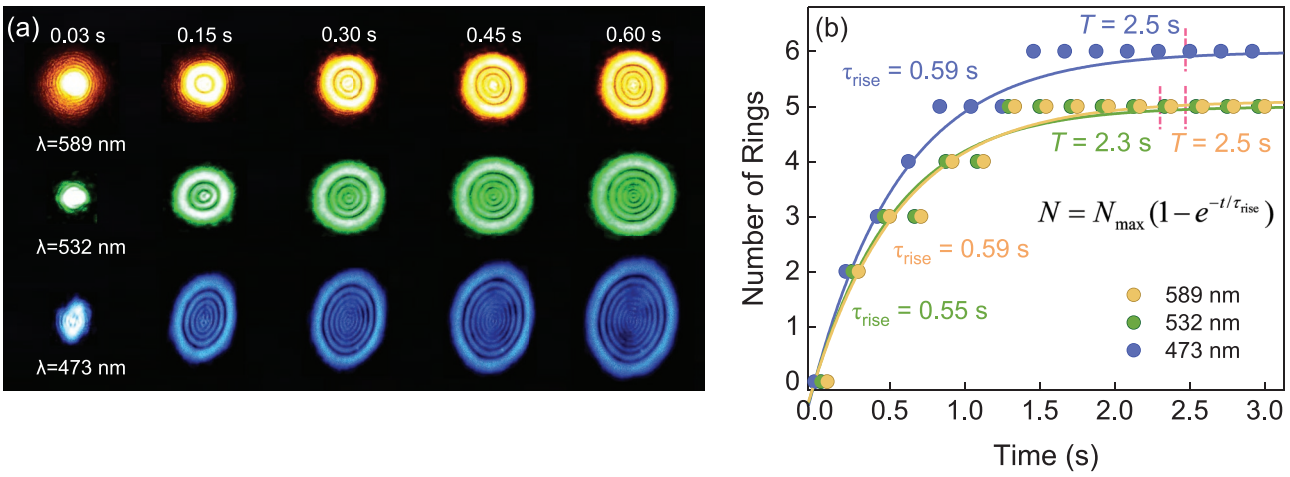

Figure 5. Formation dynamics of SSPM patterns at wavelengths of 589, 532, and 473 nm. The fluence is fixed at 90 W cm^{-2}. a) Time-sliced snapshots depicting the emergence of the rings at three wavelengths. b) Evolution of the ring numbers with time at 589, 532, and 473 nm. Solid line: exponential growth model.

In 2D layered materials, electron movement is confined in the ab plane, driven by the electrical component of the external laser beam. TaAs has an anisotropic carrier mobility, which is larger in ab plane than along the *c*-axis.[40] Thus, the electrons primarily move in the ab plane instead of along the *c*-axis, similar to the electron motion in 2D layered materials. Hence, this maintains the resultant torque. Other anisotropic electrical and optical properties of TaAs, such as the relative dielectric constant and refraction index[41] might contribute to the wind-chime model, too. Significantly, because the anisotropy in the hole mobility is not as sharp as those of electrons in 2D layered materials (for TaAs, it is reported that μ_{ab}:μ_c=2.3:1[39]), it is expected that the alignment of the flakes is relatively more time-consuming and the ring pattern formation time of TaAs is longer than that of 2D materials. This prediction is experimentally verified by the fact that the values of T for most 2D materials are reported ranging from 0.18 to 0.78 s.[3–8,11] Even after considering the laser beam intensity and flake dimensions (Equation (3)), the T values for 2D materials are significantly (we estimate it to be 3–10 times) smaller than that of the anisotropic 3D material TaAs. It is noteworthy that the thermal explanations (e.g., the thermal lens model) can hardly explain the very long pattern formation time observed for TaAs.

Since the discovery, 2D materials provide a platform for rich nonlinear optical effects[42–45] and light–matter interactions.[46–48] Our findings enrich the materials and kaleidoscope images of photonics behavior originating from laser-driven emergent coherence.

4. Conclusion

We have investigated the SSPM of a 3D Weyl semimetal (TaAs dispersion solution) at various wavelengths in the vis-NIR regime. We obtained the values of $\chi^{(3)}_{\text{one-layer}}$ at these wavelengths through SSPM, which are proportional to the absorbance. We attribute the SSPM in TaAs to laser-induced hole coherence and find that the wind-chime model and μ-dependence correlation remained effective for SSPM in this 3D material. The generalization to 3D materials with anisotropic carrier mobility, as well as the generalization from electrons to holes, facilitates the comparison of the SSPM efficiency between materials across dimensions, and aids in identifying effective materials for practical all-optical switching[3] and other photonics applications.

Supporting Information

Supporting Information is available from the Wiley Online Library or from the author.

Acknowledgements

Y.H., H.Z., and Z.L. contributed equally to this work. This work was financially supported by the Beijing Natural Science Foundation (grant no. 4191003), National Key Research and Development Program of China (grant nos. 2021YFA1400201 and 2017YFA0303603), Strategic Priority Research Program of CAS (grant no. XDB30000000), CAS Project for Young Scientists in Basic Research (grant no. YSBR-059), National Natural Science Foundation of China (grant no. 11774408), International Partnership Program of Chinese Academy of Sciences (grant no. GJHZ1826), and CAS Interdisciplinary Innovation Team.

Conflict of Interest

The authors declare no conflict of interest.

Data Availability Statement

The data that support the findings of this study are available from the corresponding author upon reasonable request.

Keywords

anisotropy, hole coherence, laser-induced phenomena, nonlinear optical response, spatial self-phase modulation, Weyl semimetals

Received: September 12, 2022
Revised: December 23, 2022
Published online: February 7, 2023

[1] S. D. Durbin, S. M. Arakelian, Y. R. Shen, *Opt. Lett.* **1981**, *6*, 411.
[2] R. Wu, Y. L. Zhang, S. C. Yan, F. Bian, W. L. Wang, X. D. Bai, X. H. Lu, J. Zhao, E. G. Wang, *Nano Lett.* **2011**, *11*, 5159.
[3] Y. L. Wu, Q. Wu, F. Sun, C. Cheng, S. Meng, J. Zhao, *Proc. Natl. Acad. Sci. USA* **2015**, *112*, 11800.
[4] Y. L. Wu, L. L. Zhu, Q. Wu, F. Sun, J. K. Wei, Y. C. Tian, W. L. Wang, X. D. Bai, X. Zuo, J. Zhao, *Appl. Phys. Lett.* **2016**, *108*, 241110.
[5] L. L. Hu, F. Sun, H. Zhao, J. Zhao, *Opt. Lett.* **2019**, *44*, 5214.
[6] W. H. Wang, Y. L. Wu, Q. Wu, J. J. Hua, J. Zhao, *Sci. Rep.* **2016**, *6*, 22072.
[7] J. D. Zhang, X. F. Yu, W. J. Han, B. S. Lv, X. H. Li, S. Xiao, Y. L. Gao, J. He, *Opt. Lett.* **2016**, *41*, 1704.
[8] Y. Jia, Y. L. Liao, L. M. Wu, Y. X. Shan, X. Y. Dai, H. Z. Cai, Y. J. Xiang, D. Y. Fan, *Nanoscale* **2019**, *11*, 4515.
[9] X. H. Li, R. K. Liu, H. H. Xie, Y. Zhang, B. S. Lyu, P. Wand, J. H. Wand, Q. Fan, Y. Ma, S. H. Tao, S. Xiao, X. F. Yu, Y. L. Gao, J. He, *Opt. Express* **2017**, *25*, 18346.
[10] X. M. Cheng, J. J. Yao, H. Zhang, X. Wang, J. T. Bai, *J., Alloy. Compd.* **2021**, *855*, 157433.
[11] Y. Jia, Y. X. Shan, L. M. Wu, X. Y. Dai, D. Y. Fan, Y. J. Xiang, *Photonics Res.* **2018**, *6*, 1040.
[12] T. Neupane, H. Wang, W. W. Yu, B. Tabibi, F. J. Seo, *Opt. Laser Technol.* **2021**, *140*, 107090.
[13] L. M. Wu, Z. J. Xie, L. L, J. L. Zhao, Y. Z. Wang, X. T. Jiang, Y. Q. Ge, F. Zhang, S. B. Lu, Z. N. Guo, J. Liu, Y. J. Xiang, S. X. Xu, J. Q. Li, D. Y. Fan, H. Zhang, *Adv. Opt. Mater.* **2018**, *6*, 1700985.
[14] J. Li, Z. L. Zhang, J. Yi, L. L. Miao, J. Huang, J. R. Zhang, Y. He, B. Huang, C. J. Zhao, Y. H. Zou, S. C. Wen, *Nanophotonics* **2020**, *9*, 2415.
[15] X. F. Han, Y. X. Weng, R. Wang, X. H. Chen, K. H. Luo, L. A. Wu, J. Zhao, *Appl. Phys. Lett.* **2008**, *92*, 151109.
[16] B. Q. Lv, H. M. Weng, B. B. Fu, X. P. Wang, H. Miao, J. Ma, P. Richard, X. C. Huang, L. X. Zhao, G. F. Chen, Z. Fang, X. Dai, T. Qian, H. Ding, *Phys. Rev. X* **2015**, *5*, 031013.
[17] X. Huang, L. Zhao, Y. Long, P. Wang, D. Chen, Z. Yang, H. Liang, M. Xue, H. Weng, Z. Fang, X. Dai, G. Chen, *Phys. Rev. X* **2015**, *5*, 031023.
[18] Z. L. Li, H. X. Chen, S. F. Jin, D. Gan, W. J. Wang, L. W. Guo, X. L. Chen, *Cryst. Growth Des.* **2016**, *16*, 1172.

[19] L. Wu, S. Patankar, T. Morimoto, N. L. Nair, E. Thewalt, A. Little, J. G. Analytis, J. E. Moore, J. Orenstein, *Nat. Phys.* **2017**, *13*, 350.
[20] H. Zhao, Q. C. An, X. Ye, B. H. Yu, Q. H. Zhang, F. Sun, Q. Y. Zhang, F. Yang, J. D. Guo, J. Zhao, *Nano Energy* **2021**, *82*, 105752.
[21] M. M. Glazov, S. D. Ganichev, *Phys. Rep.* **2014**, *535*, 101.
[22] O. Matsyshyn, U. Dey, I. Sodemann, Y. Sun, *J. Phys. D: Appl. Phys.* **2021**, *54*, 404001.
[23] Y. Gao, S. Kaushik, E. J. Philip, Z. Li, Y. Qin, Y. P. Liu, W. L. Zhang, Y. L. Su, X. Chen, H. Weng, D. E. Kharzeev, M. K. Liu, J. Qi, *Nat. Commun.* **2020**, *11*, 720.
[24] N. Sirica, R. I. Tobey, L. X. Zhao, G. F. Chen, B. Xu, R. Yang, B. Shen, D. A. Yarotski, P. Bowlan, S. A. Trugman, J. X. Zhu, Y. M. Dai, A. K. Azad, N. Ni, X. G. Qiu, A. J. Taylor, R. P. Prasankumar, *Phys. Rev. Lett.* **2019**, *122*, 197401.
[25] Q. Wu, F. Sun, Q. Y. Zhang, L. X. Zhao, G. F. Chen, J. Zhao, *Phys. Rev.* **2020**, *4*, 064201.
[26] X. H. Chen, H. T. Wang, H. J. Liu, C. Wang, G. S. Wei, C. Fang, H. C. Wang, C. Y. Geng, S. J. Liu, P. Y. Li, H. M. Yu, W. S. Zhao, J. G. Miao, Y. T. Li, L. Wang, T. X. Nie, J. Zhao, X. Wu, *Adv. Mater.* **2022**, *34*, 2106172.
[27] F. Sun, Q. Wu, Y. L. Wu, H. Zhao, C. J. Yi, Y. C. Tian, H. W. Liu, Y. G. Shi, H. Ding, X. Dai, P. Richard, J. Zhao, *Phys. Rev. B* **2017**, *95*, 235108.
[28] B. H. Yu, Z. Y. Tian, F. Sun, D. C. Peets, X. D. Bai, D. L. Feng, J. Zhao, *Opt. Express* **2020**, *28*, 15855.
[29] C. Y. Jiang, F. Sun, Z. L. Feng, S. B. Liu, Y. G. Shi, J. Zhao, *Acta Phys. Sin.* **2020**, *69*, 077801.
[30] J. Z. L. Hasaien, K. J. Zhu, F. Sun, Y. L. Wu, Y. G. Shi, J. Zhao, *Acta Phys. Sin.* **2020**, *69*, 207801.
[31] F. Sun, T. Zhang, C. J. Yi, Y. L. Wu, H. Zhao, Q. Wu, Y. G. Shi, H. Weng, J. Zhao, *Phys. Rev. B* **2021**, *104*, L100301.
[32] S. M. Chi, Z. L. Li, H. H. Yu, G. Wang, S. X. Wang, H. J. Zhang, J. Y. Wang, *Ann. Phys.* **2017**, *529*, 1600359.
[33] W. Ji, W. Z. Chen, S. H. Lim, J. Y. Lin, Z. X. Guo, *Opt. Express* **2006**, *14*, 8958.
[34] S. M. Chi, Z. L. Li, Y. Xie, Y. G. Zhao, Z. Y. Wang, L. Li, H. H. Yu, G. Wang, H. M. Weng, H. J. Zhang, J. Y. Wang, *Adv. Mater.* **2018**, *30*, 1801372.
[35] B. Xu, Y. M. Dai, L. X. Zhao, K. Wang, R. Yang, W. Zhang, J. Y. Liu, H. Xiao, G. F. Chen, A. J. Taylor, D. A. Yarotski, R. P. Prasankumar, X. G. Qiu, *Phys. Rev. B* **2016**, *93*, 121110.
[36] H. Weng, C. Fang, Z. Fang, B. A Bernevig, X. Dai, *Phys. Rev. X* **2015**, *5*, 011029.
[37] Z. Y. Tian, Q. Y. Zhang, Y. W. Xiao, G. A. Gamage, F. Tian, S. Yue, V. G. Hadjiev, J. M. Bao, Z. F. Ren, E. J. Liang, J. Zhao, *Phys. Rev. B* **2022**, *105*, 174306.
[38] M. Z. Yan, H. Q. Huang, K. N. Zhang, E. Y. Wang, W. Yao, K. Deng, G. L. Wan, H. Y. Zhang, M. Arita, H. T. Yang, Z. Sun, H. Yao, Y. Wu, S. S. Fan, W. H. Duan, S. Y. Zhou, *Nat. Commun.* **2017**, *8*, 257.
[39] D. Grassano, O. Pulci, A. M. Conte, F. Bechstedt, *Sci. Rep.* **2018**, *8*, 3534.
[40] J. Xiang, S. Hu, M. Lv, J. Zhang, H. Zhao, G. Chen, W. Li, Z. Chen, P. Sun, *J. Phys.: Condens. Matter* **2017**, *29*, 485501.
[41] R. Zu, M. Gu, L. Min, C. Hu, N. Ni, Z. Mao, J. M. Rondinelli, V. Gopalan, *Phys. Rev. B* **2021**, *103*, 165137.
[42] N. Kumar, J. Kumar, C. Gerstenkorn, R. Wang, H. Y. Chiu, A. L. Smirl, H. Zhao, *Phys. Rev. B* **2013**, *87*, 121406.
[43] Q. Wu, H. X. Zhou, Y. L. Wu, L. L. Hu, S. L. Ni, Y. C. Tian, F. Sun, F. Zhou, X. Dong, Z. Zhao, J. Zhao, *Chin. Phys. Lett.* **2020**, *37*, 097802.
[44] K. S. Novoselov, A. K. Geim, S. V. Morozov, D. Jiang, Y. Zhang, S. V. Dubonos, I. V. Grigorieva, A. A. Firsov, *Science* **2004**, *306*, 666.
[45] Z. B. Liu, X. L. Zhang, X. Q. Yan, Y. S. Chen, J. G. Tian, *Chin. Sci. Bull.* **2012**, *57*, 2971.
[46] Y. C. Tian, H. Tian, Y. L. Wu, L. L. Zhu, L. Q. Tao, W. Zhang, Y. Shu, D. Xie, Y. Yang, Z. Y. Wei, X. H. Lu, T. L. Ren, C. K. Shih, J. Zhao, *Sci. Rep.* **2015**, *5*, 10582.
[47] X. J. Wu, H. C. Wang, H. J. Liu, Y. Z. Wang, X. H. Chen, P. Chen, P. Y. Li, X. F. Han, J. G. Miao, H. M. Yu, C. H. Wan, J. Zhao, S. Chen, *Adv. Mater.* **2022**, *34*, 2204373.
[48] F. Bian, Y. C. Tian, R. Wang, H. X. Yang, H. X. Xu, S. Meng, J. Zhao, *Nano Lett.* **2011**, *11*, 3251.